PHYSICAL REVIEW A VOLUME 56, NUMBER 5 NOVEMBER 1997

Topological charge and angular momentum of light beams carrying optical vortices

M. S. Soskin, V. N. Gorshkov, and M. V. Vasnetsov
Institute of Physics, National Academy of Sciences of the Ukraine, Kiev 252650, Ukraine

J. T. Malos and N. R. Heckenberg
Department of Physics, University of Queensland, Brisbane 4072, Australia

(Received 17 March 1997)

We analyze the properties of light beams carrying phase singularities, or optical vortices. The transformations of topological charge during free-space propagation of a light wave, which is a combination of a Gaussian beam and a multiple charged optical vortex within a Gaussian envelope, are studied both in theory and experiment. We revise the existing knowledge about topological charge conservation, and demonstrate possible scenarios where additional vortices appear or annihilate during free propagation of such a combined beam. Coaxial interference of optical vortices is also analyzed, and the general rule for angular-momentum density distribution in a combined beam is established. We show that, in spite of any variation in the number of vortices in a combined beam, the total angular momentum is constant during the propagation.
[S1050-2947(97)09910-1]

PACS number(s): 42.65.Sf, 42.50.Vk

INTRODUCTION

Light beams possessing phase singularities, or wave-front dislocations [1,2] have been studied intensively in linear and nonlinear optics [3–21], to reveal their basic properties, and for the sake of possible applications. At the singularity the phase becomes undetermined and the wave amplitude vanishes, resulting in a ''dark beam'' within a light wave. Phase singularities appear on wave fronts in diffuse light scattering, when a light wave has a form of speckle field, and each speckle has one screw wave-front dislocation in the vicinity [3], also known as an optical vortex [4]. At present, several different techniques are used to generate ''singular beams:'' synthesized holograms [5,6], phase masks [7–9], active laser systems [10–13], and low-mode optical fibers [14]. Recently the generation of phase singularities was observed as a result of light wave-front deformations caused by self-action in nonlinear media [15,16].

The general result of these investigations is the origin of a new chapter of modern optics and laser physics—singular optics, which operates with terminology and laws quite new to traditional optics. Phase singularities are topological objects on wave-front surfaces, and possess topological charges which can be attributed to the helicoidal spatial structure of the wave front around a phase singularity. This structure is similar to a crystal lattice defect, and therefore was at first known as a wave-front screw dislocation [1,2]. The interference of a wave possessing such wave-front screw dislocation with an ordinary reference wave produces a spiral fringe pattern [12,17,18], or, in the case of equal wave-front curvatures, radial fringes [19]. The number of fringes radiating from the center of the interference pattern equals the modulus of the topological charge, and the direction of the spiraling is determined by the sign of the charge and relative curvature of the wave fronts.

Optical vortices embedded in a host light beam behave in some degree as charged particles. They may rotate around the beam axis, repel and attract each other, and annihilate in collision [20,21]. Other types of wave-front defects also may occur, such as edge or mixed screw-edge dislocations [22]. The possible transformations between edge and screw dislocations (in laser mode terms, 01 and doughnut modes) may be performed by modal converters [11,23,24].

The light field of a singular beam carries angular momentum [23] which may be transferred to a captured microparticle causing its rotation in a direction determined by the sign of the topological charge [25]. In nonlinear optics, so-called vortex solitons, which are singular beams in nonlinear medium, are a subject of growing interest [26,27].

However, singular beams demonstrate unusual properties even in linear optics, in free-space propagation. Optical phase singularities as morphological objects (tears of wave front) are robust with respect to perturbations. For instance, addition of a small coherent background does not destroy a vortex, but only shifts its position to another place where the field amplitude has a zero value. For vortices with multiple charge this operation will split an initially m-charged vortex into $|m|$ single-charge vortices [21]. Intuition suggests that the total topological charge would be conserved in a beam propagating in free space [1,2]. Our goal is to analyze the main properties of beams containing phase singularities in a general way, and demonstrate the limitations on the topological charge conservation principle for real beams, both theoretically and in experiment. On the basis of the present study, we establish the rules of angular-momentum transformations in light beams with phase singularities.

WAVE EQUATION SOLUTIONS POSSESSING PHASE SINGULARITIES

In this section we demonstrate some particular solutions possessing phase singularities of the scalar wave equation for a uniform isotropic medium

$$\nabla^2 E = \frac{1}{c^2}\frac{\partial^2 E}{\partial t^2}, \tag{1}$$

where E is the wave amplitude, c is the speed of light, and t is time. The existence of these solutions for a monochromatic light wave was first emphasized by Nye and Berry [1]. The derived complex amplitude of a light wave with frequency ω, wavelength λ, and wave vector $k=2\pi/\lambda$ oriented along z axis has the form

$$E(\rho,\varphi,z,t)\propto\begin{cases}\rho^{|m|}\exp(im\varphi+ikz-i\omega t), & (2a)\\ \rho^{-|m|}\exp(im\varphi+ikz-i\omega t), & (2b)\end{cases}$$

where ρ, φ, and z are cylindrical coordinates. Both solutions have a phase depending on the azimuth angle φ multiplied by an integer m (positive or negative) called the topological charge of the phase singularity (optical vortex). The wave-front (equal phase surface) forms in space part of a helicoidal surface given by the equality $m\varphi+kz=\text{const}$. After one round trip of the wave front around the z axis there is a continuous transition onto the next (or preceding) wave-front sheet separated by $m\lambda$, which results in a continuous helicoidal wave-front surface. The topological charge attributed to this wave-front structure is positive for a right-screw helicoid ($m>0$), and vice versa. In the case $|m|>1$, the wave-front structure is composed from $|m|$ identical helicoids nested on the z axis and separated by the wavelength λ.

The solutions in forms (2a) and (2b) cannot describe any real wave because of the radial amplitude dependence which grows proportionally to ρ for Eq. (2a), and tends to infinity when $\rho\to 0$ for Eq. (2b). To avoid unwanted amplitude growth, we may combine the solution in Eq. (2a) with a Gaussian beam. Using the paraxial approximation of the scalar wave equation in the form

$$\frac{1}{\rho}\frac{\partial}{\partial\rho}\left(\rho\frac{\partial E}{\partial\rho}\right)+\frac{1}{\rho^2}\frac{\partial^2 E}{\partial\varphi^2}-2ik\frac{\partial E}{\partial z}=0, \tag{3}$$

we obtain the corresponding solution for a ''singular'' wave in a Gaussian envelope carrying an optical vortex with charge m [17]:

$$E(\rho,\varphi,z)=E_s\frac{\rho_s}{w_s}\left(\frac{\rho}{w_s}\right)^{|m|}\exp\left(-\frac{\rho^2}{w_s^2}\right)\exp[i\Phi_s(\rho,\varphi,z)], \tag{4}$$

where E_s is the amplitude parameter, and ρ_s is the beam waist parameter. The phase Φ_s is

$$\Phi_s(\rho,\varphi,z)=-(|m|+1)\arctan\frac{2z}{k\rho_s^2}+\frac{k\rho^2}{2R_s(z)}+m\varphi+kz, \tag{5}$$

the transversal beam dimension is

$$w_s=\sqrt{\rho_s^2+(2z/k\rho_s)^2}, \tag{6}$$

and the radius of the wave front curvature is

$$R_s(z)=z+k^2\rho_s^4/4z. \tag{7}$$

The amplitude distribution in a transverse cross section of the beam has a form of an annulus, and the waist parameter ρ_s is connected with the radius of maximum amplitude at $z=0$ by a relation

$$\rho_{\max}=\rho_s\left(\frac{|m|}{2}\right)^{1/2}, \tag{8}$$

The maximum amplitude value of a singular wave at $z=0$, $\rho=\rho_{\max}$, therefore amounts to

$$E_{sm}=E_s\left(\frac{|m|}{2e}\right)^{|m|/2}. \tag{9}$$

The phase singularity disappears when $m=0$, and solution (4) becomes an ordinary Gaussian beam:

$$E(\rho,z)=E_g\frac{\rho_g}{w_g}\exp\left(-\frac{\rho^2}{w_g^2}\right)\exp[i\Phi_g(\rho,z)], \tag{10}$$

where the propagating parameters for Gaussian beam correspond to Eqs. (5)–(7) with $m=0$.

As an example we show that a solution in form (2b) having an amplitude singularity at $\rho\to 0$ may be used to create a solution with only a phase singularity. For this reason we take a similar solution with an amplitude singularity within Gaussian envelope,

$$E(\rho,\varphi,z)=E_s\frac{\rho_s}{\rho}\exp\left(-\frac{\rho^2}{w_s^2}\right)\exp[i\Phi_s(\rho,\varphi,z)], \tag{11}$$

where the phase Φ_s is

$$\Phi_s(\rho,\varphi,z)=\frac{k\rho^2}{2R_s(z)}+\varphi+kz. \tag{12}$$

The combination of solutions (11) and (2b) for $m=1$ removes the amplitude singularity and gives a wave which has a phase singularity at $\rho=0$:

$$E(\rho,\varphi,z)=E_s\frac{\rho_s}{\rho}\{1-\exp[-\rho^2/w_s^2+ik\rho^2/2R_s(z)]\}\times\exp(i\varphi+ikz). \tag{13}$$

The amplitude of a wave created this way is zero at the center ($\rho=0$) and decreases on periphery $\propto 1/\rho$. Other possible solutions of the scalar wave equation are Bessel beams [28] and Bessel-Gauss beams [29] carrying optical vortices.

OPTICAL VORTICES IN COMBINED BEAMS

In any practical realization of singular beams by use of synthesized holograms or special optical elements, a small coherent background is always present in a singular beam. The origin of this background may be a scattering in the direction of the singular beam propagation or readout beam diffraction by the fundamental spatial frequency of an imperfect hologram. This background causes splitting of an optical vortex with charge $|m|>1$ into $|m|$ single-charged vortices [21]. Another case is the interference between a singular wave and copropagating reference wave which is used in analyzing the value and sign of the topological charge of the phase singularity [18,21]. We shall now generalize the problem of coherent coaxial addition of singular beams carrying optical vortices with different charges (including the vortex-free wave, $m=0$). Our goal is to establish principles of to-

pological charge addition and subtraction, and revise the existing knowledge about topological charge conservation in a light beam propagating in free space.

Without loss of generality, we shall take a coaxial Gaussian wave as a coherent background for a singular wave. By varying the amplitude E_g and waist parameter ρ_g of the Gaussian beam, we may examine its influence in near and far zones, as plane or spherical waves in limiting cases. The sum of the singular beam with the coaxial Gaussian beam (or another singular beam) we shall call a combined beam.

The presence of a coherent background changes the position of a vortex which was initially localized at the center of singular beam Eq. (4). To find the positions of the vortices in the combined beam, we need to write two equations, one giving the radius of the zero-amplitude point (amplitudes of the singular and Gaussian waves are equated), and another giving the angular coordinate φ, which corresponds to the destructive interference between the singular and Gaussian waves:

$$E_g \frac{\rho_g}{w_g} \exp\left(-\frac{\rho^2}{w_g^2}\right) = E_s \frac{\rho_s}{w_s} \left(\frac{\rho}{w_s}\right)^{|m|} \exp\left(-\frac{\rho^2}{w_s^2}\right),$$

$$\Phi_g(\rho,z) = \Phi_s(\rho,\varphi,z) \pm \pi. \tag{14}$$

Equations (14) are the basis for analysis of vortex behavior in a combined beam. The first equation is easy to analyze to show the number of possible amplitude zeros in a combined beam.

To simplify the calculations, we suppose both beams have a waist at $z=0$, and use a normalized transverse coordinate $r=\rho/\rho_s$ and distance $\xi=z/L_R$, where L_R is the Rayleigh length of the singular beam, $L_R=k\rho_s^2/2$. The first equation of system (14) may be rewritten as

$$r^{|m|} = \frac{E_g}{E_s} C(\xi) \exp(\alpha r^2), \tag{15}$$

where

$$C(\xi) = (1+\xi^2)^{|m|/2} \left(\frac{1+\xi^2}{1+\xi^2/\kappa^4}\right)^{1/2}, \tag{16}$$

$$\alpha = \frac{1}{1+\xi^2} - \frac{1}{\kappa^2+\xi^2/\kappa^2}, \tag{17}$$

and κ is the ratio of waist parameters $\kappa=\rho_g/\rho_s$.

If $\alpha \leqslant 0$, Eq. (15) has only one root ($|m|$ times degenerate), as the left side is a function of r growing from zero to infinity, and the right side is a function decreasing from E_g/E_s to zero. The condition $\alpha \leqslant 0$ corresponds to the following relations for κ and ξ:

$$\kappa \geqslant 1,$$

$$\xi \geqslant \kappa, \tag{18a}$$

$$\kappa \leqslant 1,$$

$$\xi \leqslant \kappa, \tag{18b}$$

and

$$\kappa = 1,$$

$$\alpha = 0, \quad 0 < \xi < \infty. \tag{18c}$$

All zeros of amplitude in the combined beam are located at the same distance from the center. The number of zeros, n, is equal to $|m|$ and each amplitude zero is a center of a single vortex. The total topological charge is conserved in the combined beam when $\alpha \leqslant 0$.

Another situation occurs when $\alpha > 0$. The function of r in right side of Eq. (15) grows from E_g/E_s to infinity. Analysis shows three possibilities: no real roots of Eq. (15), two roots (each $|m|$ times degenerate), and one root ($2|m|$ times degenerate). The case of one root corresponds to the touching of lines representing the left and right sides of Eq. (15). This condition is determined by taking derivatives on r, which in combination with Eq. (15) gives a solution

$$\alpha r^2 = \frac{|m|}{2}, \tag{19}$$

which gives the critical ratio between the amplitude of the Gaussian beam E_g and maximum amplitude of the singular beam E_{sm}, Eq. (9):

$$\left(\frac{E_g}{E_{sm}}\right)^2_{\rm cr} = \eta_{\rm cr}^2 = \frac{1+\xi^2/\kappa^4}{1+\xi^2} \left(1 - \frac{1+\xi^2}{\kappa^2+\xi^2/\kappa^2}\right)^{-|m|}. \tag{20}$$

When the amplitude ratio $\eta = E_g/E_{sm}$ is higher than $\eta_{\rm cr}$, no vortices exist in the combined beam, as Eq. (15) has no real roots. The resulting topological charge is zero. If the ratio η is smaller than $\eta_{\rm cr}$, additional $|m|$ single-charged vortices appear with charge opposite to the original m-charged vortex, and the resulting total charge is zero again.

As the parameter α changes its sign during propagation of the combined beam both for cases $\kappa > 1$ and $\kappa < 1$, we may expect a variation in the number of vortices n in a combined beam propagating in free space, which means a change of the topological charge of the beam. Only the case $\kappa = 1$ will conserve the initial topological charge unchanged from $\xi = 0$ to infinity, independent of the beam amplitude ratio.

Figure 1 demonstrates the variation of the number of vortices in a combined beam during propagation along the ξ axis. The solid curve dividing the diagram is the dependence of $\eta_{\rm cr}$ vs ξ for a particular value of κ, $\kappa = 0.5$ [Fig. 1(a)] and $\kappa = 2$ [Fig. 1(b)]. The part of the diagram above the curve corresponds to zero number of vortices in a combined beam. In the case $\kappa < 1$ [Fig. 1(a)], the combined beam conserves topological charge until $\xi = \kappa$ ($\alpha \leqslant 0$). This area on the diagram is separated by a vertical line. Outside this region the number of vortices may vary between zero and $2|m|$, depending on the ratio η, with total topological charge equal to zero. A similar situation occurs for $\kappa > 1$, but now conservation of initial topological charge of singular beam will apply at $\xi > \kappa$ ($\alpha \leqslant 0$).

Amplitude profiles of Gaussian and singular beams are plotted in Fig. 2 for different distances ξ. The choice of parameters $m=1$, $\kappa=2$, and $\eta=1.05$ corresponds to the diagram shown in Fig. 1(b). Two points of intersection exist in a region $0 < \xi < 0.655$ (two oppositely charged vortices in the combined beam), no intersections in the region $0.655 < \xi$

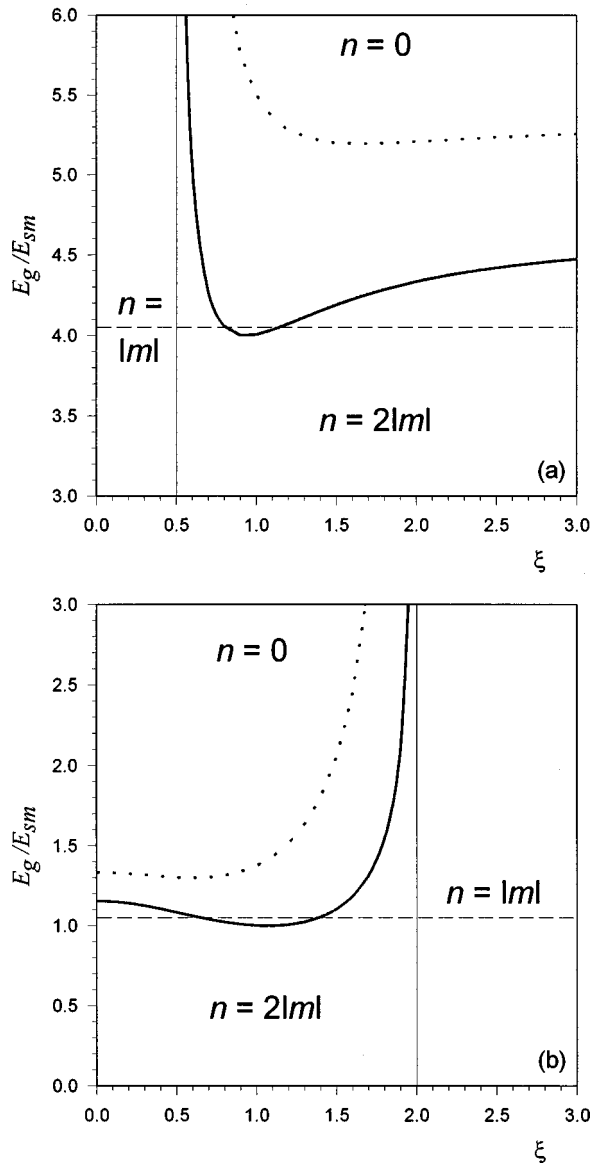

FIG. 1. Diagrams (a) and (b) show the number of vortices in a combined beam. (a) The solid curve is the dependence of the critical amplitude ratio $(E_g/E_{sm})_{\mathrm{cr}}$ on the normalized distance ξ plotted for $\kappa=0.5$ and $|m|=1$. The area above the curve contains no vortices. The region $\xi<\kappa$ separated by the vertical line contains $|m|$ vortices, and the part below the curve corresponds to $2|m|$ vortices in a combined beam. The horizontal dashed line corresponds to a particular value of the amplitude ratio, $\eta=4.05$. This line crosses in turn regions with $|m|$, $2|m|$, 0, $2|m|$ vortices. The total topological charge is m, while $\xi\leqslant\kappa$, and zero outside. (b) The same as (a), but for the case $\kappa>1$. The solid curve is a plot of η_{cr} for $\kappa=2$. The horizontal dashed line corresponds to the amplitude ratio $\eta=1.05$. For higher m values, diagrams (a) and (b) are very similar: dotted lines are plots of η_{cr} for $|m|=2$.

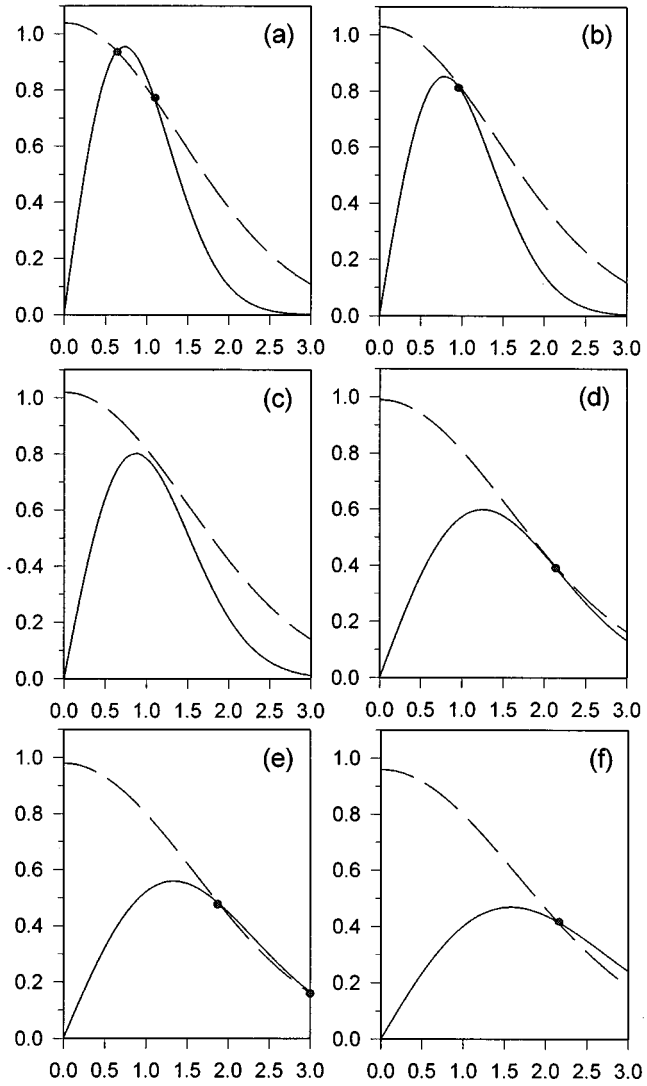

FIG. 2. Amplitude profiles of Gaussian (dashed line) and singular (solid line, $|m|=1$) waves with amplitude ratio $\eta=1.05$ and $\kappa=2$, for different normalized distances ξ. (a) $\xi=0.3$, curves intersect in two points shown by circles. (b) $\xi=0.655$, touching of the curves. (c) $\xi=1$; no intersections. (d) $\xi=1.39$, once again touching. (e) $\xi=1.5$, two intersections. (f) $\xi=2$, only the one intersection. Horizontal axis: normalized transverse coordinate r; vertical axis: wave amplitudes $E(r), E_{sm}=1$.

<1.39 (no vortices in the beam), two intersections and two oppositely charged vortices for $1.39<\xi<2$, and finally one intersection and thus a single vortex for $\xi>2$.

In a practical situation we may not have information about the initial beam amplitude ratio and waist parameters ρ_g and ρ_s, or the optical paths of beams from waist to observation plane may be different. The only experimental measured values at the plane of observation are intensity distributions of the Gaussian and singular beams. The amplitudes $A_g(\rho)$ and $A_s(\rho)$ and transversal parameters w_g and w_s may be calculated from energy distributions, and m is also easy to determine. The amplitudes necessary for existence of vortices in a combined beam may be written in this case as

$$A_g\exp\left(-\frac{\rho^2}{w_g^2}\right)=A_s\left(\frac{\rho}{w_s}\right)^{|m|}\exp\left(-\frac{\rho^2}{w_s^2}\right) \tag{21a}$$

or

$$\left(\frac{\rho}{w_s}\right)^{|m|}=\frac{A_g}{A_s}\exp\left(\frac{\rho^2}{w_s^2}-\frac{\rho^2}{w_g^2}\right), \tag{21b}$$

where A_g is the amplitude of the Gaussian beam at maximum, and A_s is connected with the maximum amplitude of

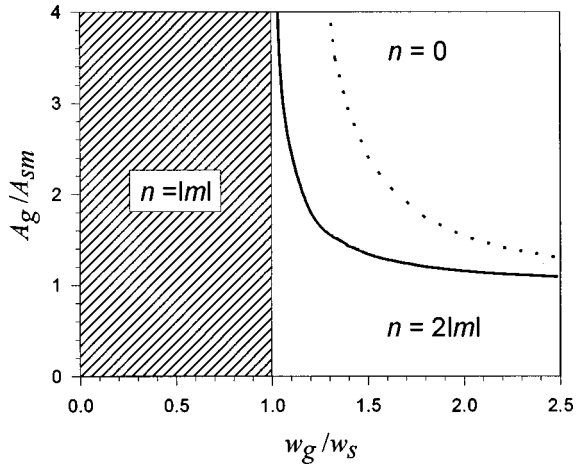

FIG. 3. Diagram showing the number of vortices in a beam combined from arbitrary Gaussian and coaxial singular beams. The horizontal coordinate is the transverse size ratio, the vertical coordinate is the amplitude ratio. The dashed area corresponds to the case of conservation of the total topological charge in the combined beam (the singular beam is wider than the Gaussian). The solid curve at the right side is the critical amplitude ratio for $|m|=1$, and the dotted curve is for $|m|=3$. The area under the curves corresponds to $2|m|$ vortices in the combined beam. No vortices are in the combined beam with parameters in the area above the curves.

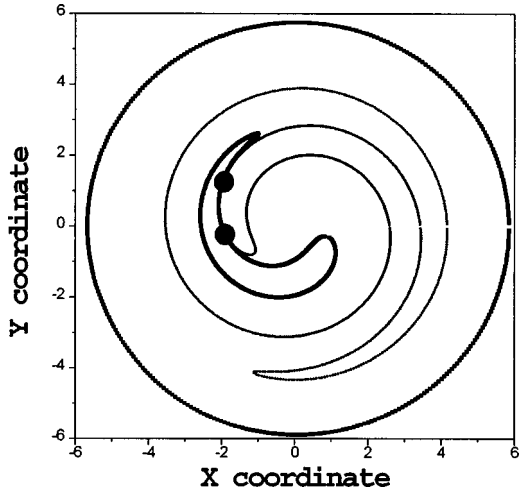

FIG. 4. Phase map shows the lines $\mathrm{Re}(E)=0$ (thick line) and $\mathrm{Im}(E)=0$ (thin line) in (x,y) coordinates normalized on ρ_s at a cross section $\xi=1.405$ of a combined beam with parameters $m=1$, $\kappa=2$, and $\eta=1.05$. Positions of vortices are shown by dots (intersections of zero lines). The original vortex is shifted from the center, and an additional vortex with opposite charge is located at the second intersection point.

the singular wave A_{sm} by the same relation as Eq. (9). Taking into account the previous analysis, we may formulate the following consequences important for experimental observation of vortex transformations in a combined beam: If the singular beam is broader than the Gaussian beam at the observation plane, $w_s>w_g$, Eq. (21b) has one $|m|$-times degenerate root, the total topological charge is conserved, and the original m-charged vortex breaks into $|m|$ vortices. If the Gaussian beam is broader than the singular, $w_g>w_s$, the total topological charge of the combined beam is zero. The number of vortices in a combined beam is determined by the relation between amplitudes. If $A_g/A_{sm}>(A_g/A_{sm})_{\mathrm{cr}}$, the combined beams will contain no vortices. If $A_g/A_{sm}<(A_g/A_{sm})_{\mathrm{cr}}$, an additional $|m|$ vortices will appear in the combined beam, as discussed above. The critical ratio $(A_g/A_{sm})_{\mathrm{cr}}$ is

$$\left(\frac{A_g}{A_{sm}}\right)_{\mathrm{cr}}=\left(\frac{w_g^2}{w_g^2-w_s^2}\right)^{|m|/2}. \tag{22}$$

The number of vortices in the combined beam for this practical situation may be determined from the diagram shown as Fig. 3. The hatched area corresponds to the case $w_s>w_g$ when the topological charge remains the same as in the singular beam. In the right part of the diagram a solid curve is plotted according to Eq. (22) for $m=1$ and a dotted curve for $m=3$. The region under the curves corresponds to the appearance of $|m|$ additional vortices and zero total topological charge. No vortices exist in the region above the corresponding curves.

To determine the position of vortices on a plane r,φ we need to use the second equation of system (14). Alternatively, we may calculate directly the position of the vortices as points of intersection of lines representing the zeros of the real and imaginary parts of the complex amplitude $E(r,\varphi,\xi)$ of the combined beam: $\mathrm{Re}(E)=0$ and $\mathrm{Im}(E)=0$ [3,15,30,31]. Figure 4 shows these lines in x,y coordinates (normalized on ρ_s) at cross section $\xi=1.405$ of a combined beam with parameters $m=1$, $\kappa=2$, and $E_g/E_{sm}=1.05$. The positions of vortices are shown by dots (intersections of zero lines). The original vortex is shifted from the center and an additional vortex with opposite charge is located at the second intersection point. Both lines $\mathrm{Re}(E)=0$ and $\mathrm{Im}(E)=0$ are closed.

Figure 5 exhibits transformations of zero-amplitude lines and corresponding vortices map for a combined beam with $m=3$, $\kappa=2$, and $\eta=1.75$. At near field ($\xi=0.5$) all vortices are suppressed by Gaussian wave with larger amplitude and waist parameter. The faster transverse spread of singular beam leads to the equalizing of amplitudes at combined beam periphery and appearance of three pairs of opposite charged vortices. Three vortices move away from the beam and disappear when $\xi=2$. Finally, when $\xi>2$, combined beam contains three single vortices located symmetrically with the conservation of the initial topological charge of the singular beam.

The trajectories of vortices within the cross section of the combined beam are shown in Fig. 6 for two main situations, $\kappa>1$ and $\kappa<1$. The combined beam ($m=1$, $\kappa=2$, and $\eta=0.5$) starts with two vortices [Fig. 6(a)] which move on their trajectories as shown in Fig. 6(a) in opposite directions, and the negative vortex leaves the beam at $\xi=2$. For another initial amplitude ratio $\eta=1.05$, the behavior of the vortices is somewhat different. Two vortices annihilate in collision at $\xi\approx 0.655$ [Fig. 6(b)], and then the beam does not contain any singularity until $\xi\approx 1.39$. Born as a pair, two new vortices with opposite charges repel each other and finally one (negatively charged) disappears at infinity ($r\to\infty$) at $\xi=2$, and the remaining one carries the initial charge of the singular beam. In the case $\kappa<1$ the combined beam ($m=1$, $\kappa=0.5$, and $\eta=4.05$) starts with only the primary vortex (shifted from the center), and an additional negative vortex enters the beam at

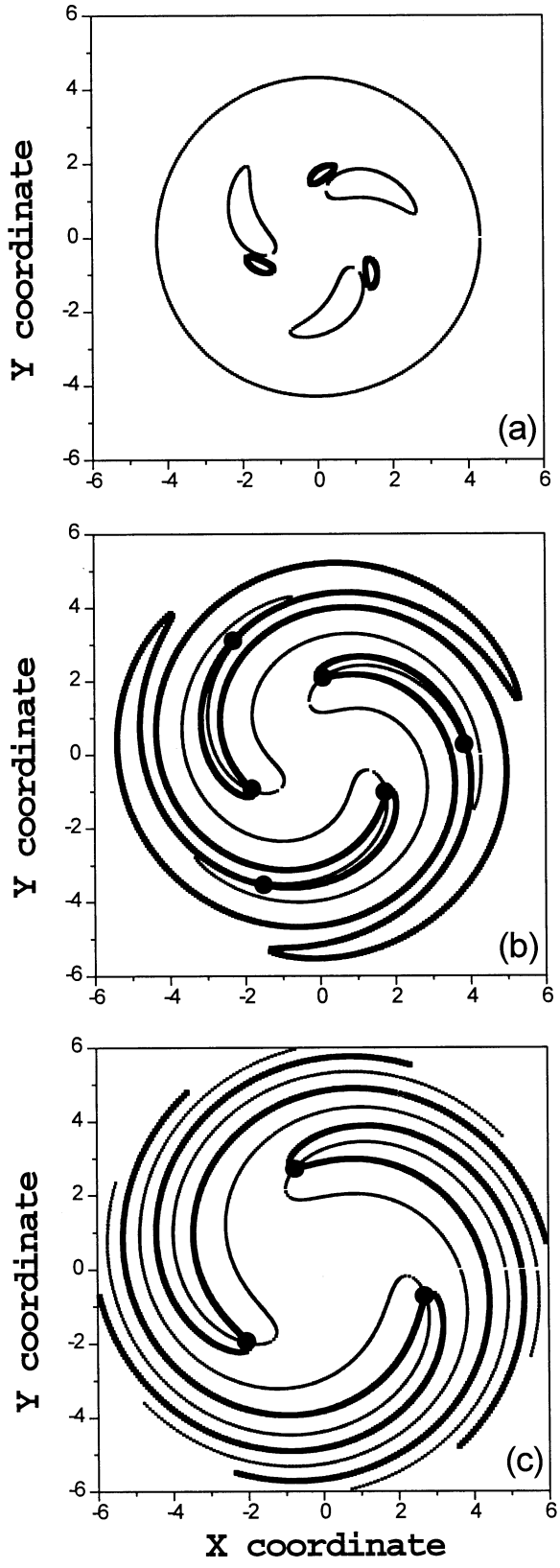

FIG. 5. Phase maps for different distances ξ of a combined beam propagation with parameters $m=3$, $\kappa=2$, and $\eta=1.75$. (a) $\xi=0.5$, lines $\mathrm{Re}(E)=0$ and $\mathrm{Im}(E)=0$ do not intersect, and no vortices exist in the combined beam. (b) $\xi=1.25$, lines $\mathrm{Re}(E)=0$ and $\mathrm{Im}(E)=0$ intersect in points shown by dots, and six single-charged vortices (three pairs) exist in the beam. (c) $\xi=2.5$, three intersection points are shown by dots, and three vortices are located symmetrically around the beam center.

$\xi=0.5$ coming from infinity [Fig. 6(c)]. After several round trips it meets the prime vortex, and both annihilate in collision at $\xi\approx 0.81$. A new vortices pair originates at $\xi\approx 1.16$, and exists within the beam up to infinity.

The analysis of vortex behavior in a beam combined from two coaxial singular beams may be performed in a similar manner. However, the combined beam may possess some new features in this case. First, both beams have zero amplitude at the center. If $|m_1|\neq|m_2|$, the combined beam will have at the center a vortex with the smaller absolute value of the charge. On the beam periphery, depending on the ratios of amplitudes and sizes, the number of vortices may vary between zero, $|m_1-m_2|$, and 2 $|m_1-m_2|$. In the particular case when $|m_1|=|m_2|$, there are two situations: $m_1=m_2$ and $m_1=-m_2$. When charges have the same sign, waves add coherently producing circular interference fringes [32], and the only m-charged vortex is located at the beam center. When vortices have opposite charges, they compete with each other for the central position. For small ρ, we may neglect the Gaussian envelope of the beams, and write the amplitude at the core as

$$E(\rho,\varphi)\propto\rho^{|m|}[A_{s1}e^{im\varphi}+A_{s2}e^{-im\varphi}], \tag{23}$$

which determines the phase near the core as $\arctan[(A_{s1}-A_{s2})/(A_{s1}+A_{s2})\tan(m\varphi)]$. This means that the vortex with larger host wave amplitude will win, but becomes anisotropic [30]. Finally, if $A_{s1}=A_{s2}$, vortices annihilate each other. The interference pattern displays $2|m|$ fringes radiating from the center.

EXPERIMENTAL OBSERVATION OF VORTICES IN COMBINED BEAM

The setup for our experiment is shown in Fig. 7. The linearly polarized output beam of a 10-mW He-Ne laser operating on the TEM_{00} mode is split first at beamsplitter BS1. The directly transmitted beam is diffracted at the holographic grating, and the first diffracted order (singular beam) is selected with the iris aperture. The holographic gratings are phase holograms restoring charge -1 and 3 singular beams, both blazed for greatest efficiency into first order [25]. The reflected beam from beamsplitter BS1 is further split at BS2 into the ''background'' Gaussian beam (reflected beam) and reference wave (transmitted beam). Lenses $L1-L4$ are used to control the sizes and radii of curvature of the Gaussian and reference wave. Lens $L2$ is finely controlled with a translation stage to allow fine adjustments of the wave-front curvature. Polarizing beamsplitters (PBS's) are used to control the relative intensities of the singular and Gaussian beams. BS3 recombines the singular and Gaussian beams, and BS4 interferes with the combined beam and the reference wave. (Double reflection of the singular beam from BS3 and mirror M does not change the sign of its topological charge.) Finally, lens $L5$ creates a magnified image of the beam on the screen, recorded with a charge-coupled device (CCD) camera.

The experimental technique consisted, first, of an alignment of the singular and Gaussian beams to make them coaxial. The resulting interference pattern, observed in the far field, was then used to determine the relative difference in curvature of wave fronts between the two beams. This was

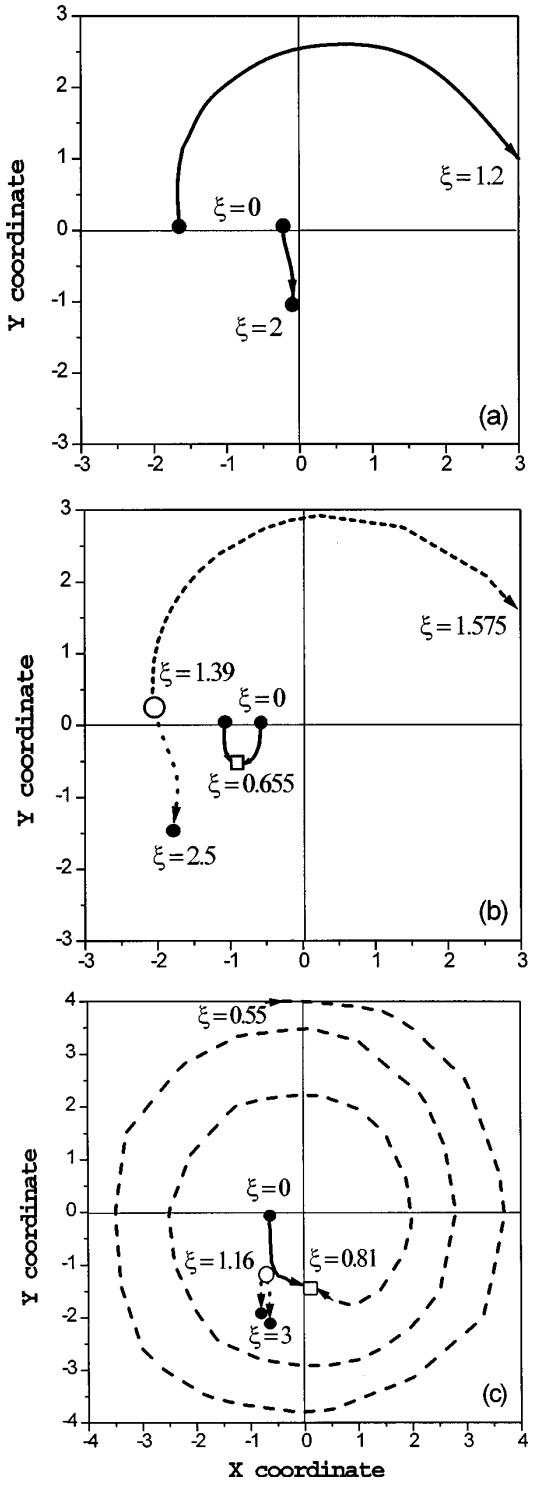

FIG. 6. Vortex trajectories in a combined beam cross section. (a) For $m=1$, $\kappa=2$, and $\eta=0.5$. The combined beam starts with two oppositely charged vortices shown by dots. The negative vortex leaves the beam at $\xi=2$. (b) Two vortices in a beam with $\eta=1.05$ annihilate in collision at $\xi\approx0.655$. A pair of two new vortices with opposite charges appear at $\xi\approx1.39$. They repel each other and finally one (negatively charged, dashed line) disappears at infinity ($r\to\infty$) at $\xi=2$. (c) Combined beam ($m=1$, $\kappa=0.5$, $\eta=4.05$) starts with only the primary vortex (shifted from the center), and an additional negative vortex enters the beam at $\xi=0.5$ (dashed line) coming from infinity. After several round trips it meets the prime vortex, and both annihilate in collision at $\xi\approx0.81$. New vortices' pair originates at $\xi\approx1.16$ (dotted lines).

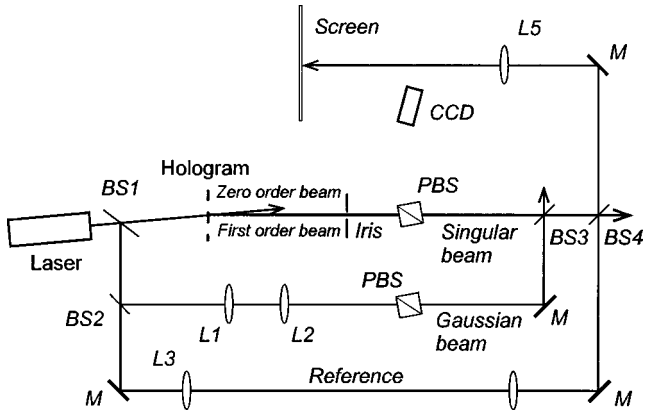

FIG. 7. Sketch of the experimental setup. The He-Ne laser beam splits into three channels. In the first channel a singular beam is created by the hologram, the second channel carries the Gaussian wave, and the reference wave is formed in the third channel. The interference patterns are observed on a screen.

adjusted using the position of lens $L2$, so that there was at most one round of dark fringe in the pattern. At this point, the wavefronts of two beams were effectively matched at the observation screen.

The profiles of energy distribution in the Gaussian and singular beams were obtained from separate CCD images, and the relative adjustment in beam intensities using PBS's could then be carried out to obtain the necessary number of amplitude graph intersection points. The corresponding intensity distributions are shown in Figs. 8 and 9 for Gaussian and singular beams (charges -1 and 3). Once the two beams were roughly the required relative intensity and size for additional vortices to be observable, the reference wave was used to interfere the intensity pattern to observe the presence of fringe dislocations, and hence the vortices in the original pattern.

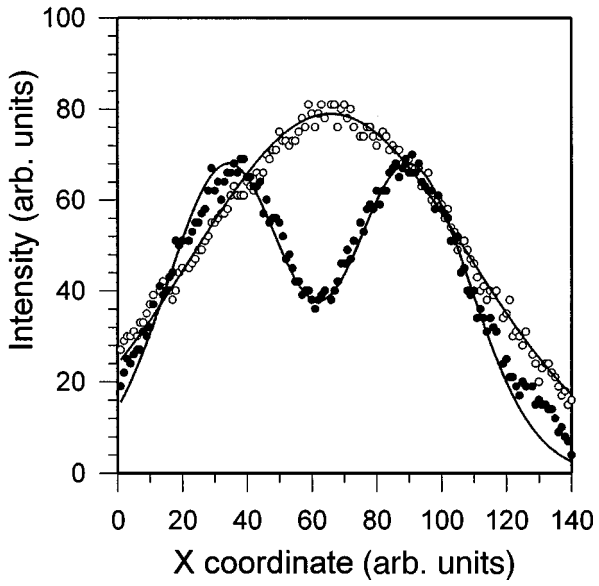

FIG. 8. Experimental intensity distributions for Gaussian ($m=0$, open circles) and singular ($m=-1$, closed circles) beams at the observation plane. Solid lines are numerical fits according to formulas (24).

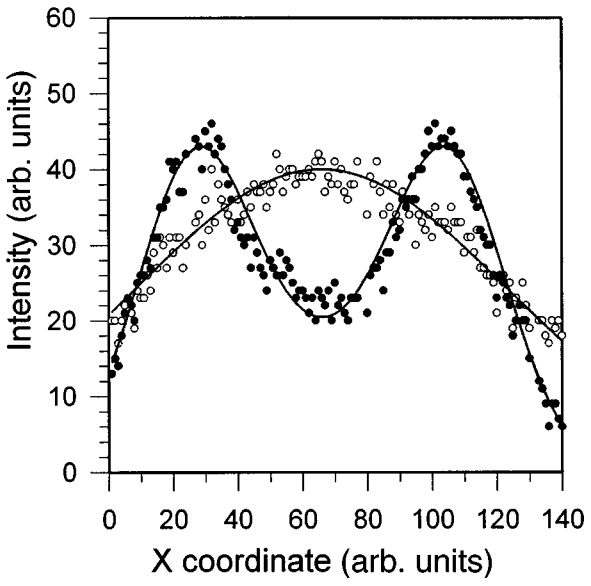

FIG. 9. The same distributions as in Fig. 8, for Gaussian and charge 3 singular beams.

The reference beam was simply adjusted through the choice of lenses $L3$ and $L4$ to be of much larger size than the combined beam cross section. The interference picture produced by the superposition of the reference beam and the combined beam at BS4 could be roughly controlled to give a reasonable number of fringes for sufficient resolution of any fringe dislocations present. To avoid reduction of fringe visibility due to a loss of coherence through multilongitudinal mode operation of the laser, all path differences were made integer multiples of the laser cavity length.

The parameters obtained from a numerical fit of the data were used for a comparison of the experimental results with theoretical predictions. The following functions were used to generate the intensity profiles of Gaussian and singular beams numerically:

$$P_g(x)=\left\{A_g\ \exp\left[-\frac{(x-x_0)^2}{w_g^2}\right]\right\}^2,$$

$$P_{-1}(x)=\left\{\frac{A_{-1}}{w_{-1}}\left[(x-x_0)^2+y_0^2\right]^{1/2}\exp\left[-\frac{(x-x_0)^2+y_0^2}{w_{-1}^2}\right]\right\}^2,$$

$$P_3(x)=\left\{\frac{A_3}{w_3^3}\left[(x-x_0)^2+y_0^2\right]^{3/2}\exp\left[-\frac{(x-x_0)^2+y_0^2}{w_3^2}\right]\right\}^2, \tag{24}$$

where A_g, A_{-1}, and A_3 are the amplitudes of the respective waves (Gaussian, singular charges -1 and 3) and w_g, w_{-1}, and w_3 are the beam sizes. The function $P_g(x)$ is the intensity profile of a Gaussian beam defined in the x,y plane, where the profile is taken along the x direction with $y=0$. $P_{-1,3}$ are the intensity profiles along x axis of singular beams, charges -1 and 3, at $y=y_0$, in order to take into account a small misalignment of the beam centers, which prevents the central minimum of the singular beam from going to zero. Parameters x_0 and y_0 determine the beam center. The data obtained from the CCD (in relative units) were fitted to functions (24) with fitting parameters: A_g $=8.86$, $w_g=85.22$, and $x_0=65.76$ for the Gaussian beam, and $A_{-1}=19.23$, $(A_{-1m}=8.25)$, $w_{-1}=45.81$, $x_0=62.25$, and $y_0=16.73$ for the singular (charge -1) beam. The calculated curves are shown in Fig. 8 (solid lines). The ratio of the beam sizes is $w_g/w_s=1.86$, i.e., the Gaussian beam is wider than the singular. The amplitude ratio is A_g/A_{-1m} $=1.07$, and according to the theoretical predictions (see the diagram in Fig. 3) an additional vortex should appear in the combined beam with a sign opposite to the original vortex. The presence of intersection points of the curves also indicates two vortices existence in the combined beam.

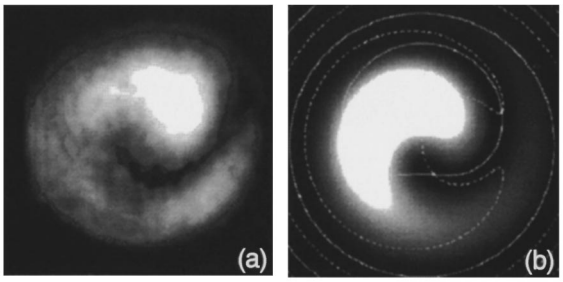

FIG. 10. Experimental (a) and numerically generated (b) intensity distributions in a combined (Gaussian plus $m=-1$ singular) beam cross section. Zero-amplitude lines are shown in (b), when the solid line represents the real part of the complex amplitude, and the dashed line the imaginary part.

For the profiles of the Gaussian and charge 3 singular beam, the fitting parameters were $A_g=6.29$, $w_g=115.92$, and $x_0=66.30$ for the Gaussian beam, and $A_3=15.82$ $(A_{3m}$ $=6.49)$, $w_3=41.23$, $x_0=66.05$, and $y_0=33.91$ for the singular beam (Fig. 9). The Gaussian beam is again wider than the singular, and the amplitude ratio corresponds to the case of three additional vortices appearing, with the total topological charge of the combined beam being zero.

For the two superpositions investigated, namely, Gaussian beam with charge -1 singular and Gaussian with charge 3 singular, the intensity patterns were calculated in gray scale and are shown in Figs. 10 and 11. To generate the two-dimensional intensity distribution $I(x,y)$ in a beam combined from Gaussian and charge -1 singular beams numerically, the expression for $I(x,y)$ is represented as follows:

$$I(x,y)=P_g(x,y)+P_{-1}(x,y)+2\sqrt{P_g(x,y)P_{-1}(x,y)}\times\cos\left(\frac{x^2+y^2}{R^2}-\arctan\frac{y}{x}+\delta\right), \tag{25}$$

where R is the radius of relative curvature of the Gaussian wave front with respect to the singular wave, δ is an adjustable phase factor, and $\arctan(y/x)$ is the azimuth angle. The intensity distribution for the combined beam with Gaussian and charge 3 singular wave has the same form as Eq. (25), only the azimuth factor becomes $3\arctan(y/x)$. Figures 10 and 11 also show the experimental patterns of combined beam intensity in the far field and calculated intensity distributions with lines of zeros for the functions $\mathrm{Re}[E(x,y)]=0$ (solid line) and $\mathrm{Im}[E(x,y)]=0$ (dashed line). The points of intersection of the zero lines correspond to the positions of vortices. For the case of the combination of a Gaussian and a

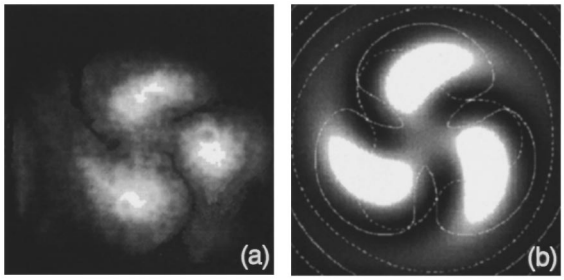

FIG. 11. The same intensity distributions as in Fig. 10, but for Gaussian plus $m=3$ singular combined beam.

charge -1 singular beam, a single dark spiral fringe is seen [Fig. 10(a)]. The curved shape of the fringe is due to slight difference in wave-front curvature. The zero-amplitude lines have two points of intersection, corresponding to two vortices existing within the dark fringe [Fig. 10(b)]. For the Gaussian and charge 3 singular beam, three dark fringes radiating from the center of the pattern are present [Fig. 11(a)]. There are six intersection points of the zero lines in Fig. 11(b), indicating two vortices with opposite charges located in each dark fringe.

To demonstrate the existence of vortices in the combined beams clearly, the interference patterns of the combined beam with the reference wave are shown in Figs. 12 and 13. The results of experimental observations are compared with calculated intensity distributions. For the Gaussian and charge -1 combined beam, both theory and experiment show a dark spiral fringe which begins at the center of the pattern and ends after nearly two turns [Figs. 12(a) and 12 (b)]. Thereafter, the interference fringes form rings corresponding well with the theory: the phase has no rotating component at this area. Thus two oppositely charged vortices make the total topological charge zero.

For the Gaussian and charge 3 combined beam, there are three inner interference ''forks,'' equally separated by 120° and directed clockwise, and three outer ''forks'' directed anticlockwise (Fig. 13). Hence there are six single vortices altogether, or three pairs of oppositely charged vortices. At the area outside, the fringes again form rings.

The experimental observations clearly demonstrate the appearance of additional vortices in combined beams, changing the total topological charge of a beam. We have thus shown in both theory and experiment that the topological charge of a beam containing phase singularities is not a constant while propagating in free space.

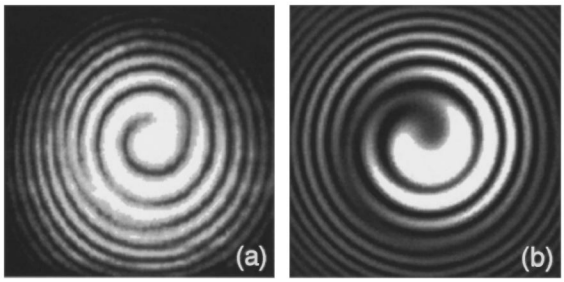

FIG. 12. The interference pattern of the combined beam (Gaussian plus $m=-1$ singular) and reference wave. The primary vortex is located near the center, and an additional vortex is seen with positive charge: (a) experimental picture; (b) numerical simulation.

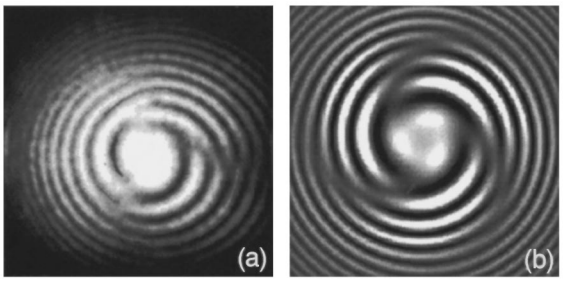

FIG. 13. The interference pattern of the combined beam (Gaussian plus $m=3$ singular) and reference wave. The primary vortex is split into three vortices, and an additional three vortices with negative charge produce, with them, three pairs: (a) experimental picture; (b) numerical simulation.

ANGULAR MOMENTUM OF LIGHT BEAM CARRYING OPTICAL VORTICES

The rotation of phase around the vortex axis causes a nonzero value of angular momentum of a beam [23,33]. The origin of the angular momentum may be easy explained from simple evaluations. As the wave front of a singular beam has a helicoidal shape, the Poynting vector $P(\rho,\varphi,z)$ which is perpendicular to the wave front surface has at each point a nonzero tangential component. In the paraxial approximation this component equals $P_{\perp}(\rho,\varphi,z)=-mP/k\rho$, and the angular-momentum density in the z-axis direction is $M_z(\rho,\varphi,z)=(\rho/c^2)P_{\perp}(\rho,\varphi,z)$. As the Poynting vector is proportional to a light wave intensity, $P\propto|E_s(\rho,\varphi,z)|^2$, we may obtain the expression for angular-momentum density of a singular beam:

$$M_z(\rho,\varphi,z)\propto -m|E_s(\rho,\varphi,z)|^2. \tag{26}$$

The time-averaged density of angular momentum directed along the z axis in a combined beam cross section may be calculated in a general form [23,33] as

$$M_z=\frac{i}{2}\,\omega\epsilon_0\left[x\left(E^*\,\frac{\partial E}{\partial y}-E\,\frac{\partial E^*}{\partial y}\right)-y\left(E^*\,\frac{\partial E}{\partial x}-E\,\frac{\partial E^*}{\partial x}\right)\right], \tag{27}$$

where ϵ_0 is the permittivity of free space. The total angular momentum L_z of the beam is an integral over the beam cross section

$$L_z=\int_{-\infty}^{\infty}\int_{-\infty}^{\infty}M_z dx\,dy. \tag{28}$$

The simplest combined beam is a sum of singular [Eq. (4)] and Gaussian [Eq. (10)] beams, and its angular momentum calculated according to Eq. (27) is

$$\begin{aligned}M_z(\rho,\varphi,z)=&-\omega\epsilon_0 m\{|E_s(\rho,\varphi,z)|^2\\&+|E_s(\rho,\varphi,z)E_g(\rho,z)|\cos[\Phi_s(\rho,\varphi,z)\\&-\Phi_g(\rho,z)]\},\end{aligned} \tag{29}$$

which attains a simple form for a pure singular beam ($E_g=0$):

$$M_z(\rho,\varphi,z)=-\omega\epsilon_0 m|E_s(\rho,\varphi,z)|^2, \tag{30}$$

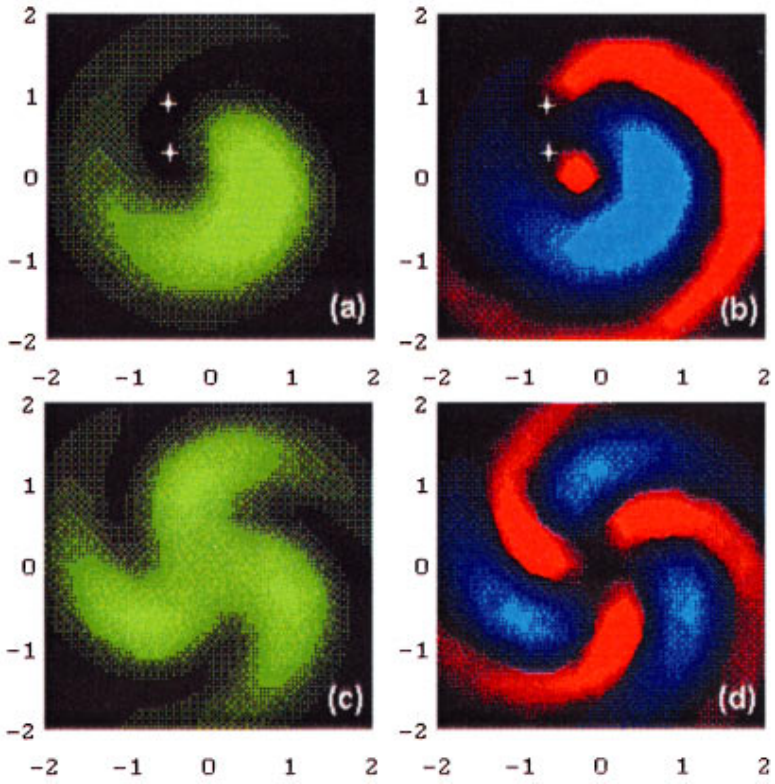

FIG. 14. (Color) Distribution of energy and angular momentum in a combined beam. (a) and (b) $m=1$, $E_g/E_{sm}=1.05$, $\kappa=2$, and $\xi=0.3$. Green is for energy distribution, red for positive angular momentum density $M_z>0$, and blue for negative angular-momentum density $M_z<0$. The positions of two oppositely charged vortices are shown by white crosses. (c) and (d) The same distributions for $m=3$, $E_g/E_{sm}=2.5$, and $\kappa=2$. No vortices exist in the combined beam with this amplitude ratio, but a modulation of the angular-momentum density is clearly seen. The transverse coordinates are x and y, normalized on ρ_s.

coinciding with Eq. (26), and

$$L_z=-2\pi\omega\epsilon_0 m E_s^2\left(\frac{\rho_s}{w_s}\right)^2\int_0^\infty \rho d\rho\left(\frac{\rho}{w_s}\right)^{2|m|}\exp\left(-\frac{2\rho^2}{w_s^2}\right)$$

$$=-\frac{\pi m|m|!}{2^{|m|+1}}\,\omega\epsilon_0\rho_s^2E_s^2. \tag{31}$$

The density of the angular momentum of a singular beam M_z is therefore proportional to the beam intensity, and the total angular momentum L_z to the beam energy. In a medium without losses, the total momentum L_z is conserved, as well as the beam energy.

The relation obtained for the angular momentum of a combined beam (29) may be generalized as a law of coaxial addition of N beams carrying optical vortices with topological charges m_i:

$$M_z(\rho,\varphi,z)=-\frac{\omega\epsilon_0}{2}\sum_{i,j}^{N}(m_i+m_j)|E_i(\rho,\varphi,z)E_j(\rho,\varphi,z)|$$

$$\times\cos[\Phi_i(\rho,\varphi,z)-\Phi_j(\rho,\varphi,z)]. \tag{32}$$

This law is valid not only for singular waves with a Gaussian envelope, but for all kinds of waves with axially symmetric amplitude distributions.

An interesting consequence following from Eq. (29) is that even a small amount of a singular wave combined with a strong Gaussian wave produces a substantial modulation of the angular-momentum density. Figure 14 represents the calculation of angular-momentum density of combined beams with parameters $m=1$, $\kappa=2$, and $\eta=1.05$ (a) and $m=3$, $\kappa=2$, and $\eta=2.5$ (b).

For a combined beam with a density of angular-momentum distribution given by Eq. (29), the total angular momentum is equal to that of the singular beam alone, because an interference term gives a zero amount in integral (28). This demonstrates that coherent addition of a wave with zero angular momentum does not affect the resulting angular momentum of the combined beam. Using the general form of the angular-momentum distribution in a combined beam (32), we are able now to calculate the result of coaxial interference of N arbitrary singular beams,

$$L_z=\sum_i^N L_{zi}, \tag{33}$$

which establishes a rule: In a beam combined from N coaxial beams, the angular momenta L_{zi} add arithmetically.

This rule gives interesting consequences for the addition of singular beams with equal and opposite topological charges. Two identical singular beams with equal energy but opposite charges form a vortex-free beam with zero angular momentum, independent of the phase relation between them. Identical beams with equal topological charges of vortices do not obey the general rule (33), because the interference term is a constant in this case, and the energy of the summed

beam is strongly dependent on relative phases of components. Further, adding a vortex-free wave with zero angular momentum cannot change the total angular momentum L_z of a beam, even though it may suppress all the vortices in the combined beam.

To understand the transformations of angular momentum associated with an m-charged vortex in a combined beam where the number of vortices may change and even become zero, we need to imagine the wave front of a combined beam which is not a symmetrical m-pitched helicoid as for a pure singular beam. When all the vortices are suppressed by the strong background wave, the wave front of the combined beam still has folds, but is a smooth surface without defects. The inclination of local ''rays'' which are perpendicular to the surface produces both positive and negative components of the angular momentum. With an increase of Gaussian background wave amplitude, the folds become smaller, but the beam amplitude grows proportionally, and resulting negative and positive parts of angular momentum have nearly the same value. The difference between the negative and positive components of the angular momentum remains exactly equal to the initial angular momentum of the singular beam, but is now due to small residual amplitude modulation over the combined beam cross section. In the case of multiple vortices localized within a combined beam, the distribution of the angular momentum becomes more complicated, but the resulting total angular momentum remains constant.

CONCLUSIONS

Our analysis of coherent coaxial addition of optical waves carrying (at least one) optical vortices has revealed the general properties of combined beams. We have studied in detail the behavior of vortices in a beam combined from singular and ''background'' Gaussian waves in order to check the principle of topological charge conservation. In brief, we obtained the following results.

(1) Addition of a coherent coaxial vortex-free wave to a singular wave with a m-charged vortex may change the number of vortices and the total topological charge in the combined beam. Depending on background wave parameters, the number of vortices in the combined beam may vary between zero, $|m|$, and $2|m|$. The total topological charge is m or zero.

(2) In free-space propagation from $z=0$ to infinity, the total topological charge and number of vortices in a combined beam do change for any choice of background wave parameters, except the case $\kappa=1$ (equal transverse sizes).

(3) We demonstrate for the first time to our knowledge, the possibility, in free-space propagation, of additional vortices appearing from the far periphery of a beam (from infinity), and their disappearance at a beam periphery.

(4) The obtained results are also applicable to the case of combinations of singular beams.

(5) We show that the total angular momentum of a beam is conserved in all cases in free-space propagation, in contrast with the total topological charge. We establish the main rules for addition and subtraction of angular momenta of light beams.

(6) We analyzed the transverse distribution of the angular momentum in a combined beam cross section, and found a strong spatial modulation of the angular-momentum density even in the case of absence of vortices in a combined beam.

ACKNOWLEDGMENTS

This research was supported, in part, by the International Science Foundation, and by the Australian Department of Industry, Science and Tourism.

[1] J. F. Nye and M. V. Berry, Proc. R. Soc. London, Ser. A **336**, 165 (1974).
[2] M. V. Berry, in *Les Houches Lecture Series Session XXXV*, edited by R. Balian, M. Klaéman, and J.-P. Poirier (North-Holland, Amsterdam, 1981), p. 453.
[3] N. B. Baranova, A. V. Mamaev, N. F. Pilipetskii, V. V. Shkunov, and B. Ya. Zel'dovich, J. Opt. Soc. Am. **73**, 525 (1983).
[4] P. Coullet, L. Gil, and F. Rocca, Opt. Commun. **73**, 403 (1989).
[5] V. Yu. Bazhenov, M. V. Vasnetsov, and M. S. Soskin, Pis'ma Zh. Eksp. Teor. Fiz. **52**, 1037 (1990) [JETP Lett. **52**, 429 (1990)].
[6] N. R. Heckenberg, R. McDuff, C. P. Smith, H. Rubinsztein-Dunlop, and M. J. Wegener, Opt. Quantum Electron. **24**, S951 (1992).
[7] S. N. Khonina, V. V. Kotlyar, M. V. Shinkarev, V. A. Soifer, and G. V. Uspleniev, J. Mod. Opt. **39**, 1147 (1992).
[8] S. Tidwell, G. Kim, and W. Kimura, Appl. Opt. **32**, 5222 (1993).
[9] M. W. Beijersbergen, R. P. C. Coerwinkel, M. Kristiensen, and J. P. Woerdman, Opt. Commun. **112**, 321 (1994).
[10] J. M. Vaughan and D. V. Willetts, J. Opt. Soc. Am. **73**, 1018 (1983).
[11] C. Tamm and C. O. Weiss, J. Opt. Soc. Am. B **7**, 1034 (1990).
[12] F. T. Arecchi, G. Giacomelli, P. L. Ramazza, and S. Residori, Phys. Rev. Lett. **67**, 3749 (1991).
[13] S. R. Liu and G. Indebetouw, J. Opt. Soc. Am. B **9**, 1507 (1992).
[14] M. Ya. Darsht, I. V. Kataevskaya, N. D. Kundikova, and B. Ya. Zel'dovich, Zh. Eksp. Teor. Fiz. **107**, 1 (1995) [Sov. Phys. JETP **80**, 817 (1995)].
[15] A. V. Ilyenkov, A. I. Khizniak, L. V. Kreminskaya, M. S. Soskin, and M. V. Vasnetsov, Appl. Phys. B **62**, 465 (1996).
[16] T. Ackemann, E. Kriege, and W. Lange, Opt. Commun. **115**, 339 (1995).
[17] V. Yu. Bazhenov, M. S. Soskin, and M. V. Vasnetsov, J. Mod. Opt. **39**, 985 (1992).
[18] A. G. White, C. P. Smith, N. R. Heckenberg, H. Rubinsztein-Dunlop, R. McDuff, C. O. Weiss, and Chr. Tamm, J. Mod. Opt. **38**, 2531 (1991).
[19] O. Bryngdahl, J. Opt. Soc. Am. **63**, 1098 (1973).
[20] G. Indebetouw, J. Mod. Opt. **40**, 73 (1993).
[21] I. V. Basistiy, V. Yu. Bazhenov, M. S. Soskin, and M. V.

Vasnetsov, Opt. Commun. **103**, 422 (1993).
[22] I. V. Basistiy, M. S. Soskin, and M. V. Vasnetsov, Opt. Commun. **119**, 604 (1995).
[23] M. W. Beijersbergen, L. Allen, H. E. L. O. van der Ween, and J. P. Woerdman, Opt. Commun. **96**, 122 (1993).
[24] E. Abramochkin and V. Volostnikov, Opt. Commun. **83**, 123 (1991).
[25] H. He, N. R. Heckenberg, and H. Rubinsztein-Dunlop, J. Mod. Opt. **42**, 217 (1995).
[26] G. Swartzlander, Jr. and C. Law, Phys. Rev. Lett. **69**, 2503 (1992).
[27] B. Luther-Davies, R. Powles, and V. Tikhonenko, Opt. Lett. **19**, 1816 (1994).
[28] J. Durnin, J. Opt. Soc. Am. A **4**, 651 (1987).
[29] F. Gori, G. Guatari, and C. Padovani, Opt. Commun. **64**, 491 (1987).
[30] I. Freund, N. Shvartsman, and V. Freilikher, Opt. Commun. **101**, 247 (1993).
[31] N. R. Heckenberg, M. Vaupel, J. T. Malos, and C. O. Weiss, Phys. Rev. A **54**, 2369 (1996).
[32] M. Harris, C. A. Hill, and J. M. Vaughan, Opt. Commun. **106**, 161 (1994).
[33] L. Allen, M. W. Beijersbergen, R. J. C. Spreeuw, and J. P. Woerdman, Phys. Rev. A **45**, 8185 (1992).